Applied Surface Science 729 (2026) 166230

Contents lists available at ScienceDirect

Applied Surface Science

journal homepage: www.elsevier.com/locate/apsusc

Full Length Article

Thermochromic behavior of Ta-doped VO_2 thin films: Influence of configuration, pulsed oxygen and dopant ratio

A. Casas-Acuña [a,b], A.J. Santos [a,b,*], N. Martin [c], J.J. Jiménez [a,b], M. Garzón [a,b], R. García [a,b], F.M. Morales [a,b]

[a] IMEYMAT: Institute of Research on Electron Microscopy and Materials of the University of Cádiz, E-11510 Puerto Real, Spain
[b] Department of Materials Science and Metallurgic Engineering, and Inorganic Chemistry, Faculty of Sciences, University of Cádiz, E-11510 Puerto Real, Spain
[c] SUPMICROTECH, CNRS, Institut FEMTO-ST, 25000 Besançon Cedex, France

ARTICLE INFO

Keywords:
Smart windows
Vanadium dioxide
Ta-doping
Glancing angle co-deposition
Rapid thermal annealing
UV–Vis-NIR spectrophotometry
Thermochromic behavior

ABSTRACT

This study focuses on the optimization of the optical performance of thermochromic vanadium dioxide (VO_2) films doped with tantalum. $V_xTa_{1-x}O_2$ layers of nominal thickness 50 nm were deposited on glass by co-sputtering of V and Ta in glancing-angle geometry, and subsequent fast annealing in air. The impact of the deposition configuration, either a $V_{0.973}Ta_{0.027}O_y$ monolayer or alternating $VO_y/V_{0.916}Ta_{0.084}O_y$ multilayers, and the optional coupling of reactive oxygen pulses (t_{ON} = 0, 4, 8 s) was studied for different Ta/V atomic ratios (1, 2.7, 3, and 5Ta). The longest oxygen injection times allow to achieve films with lower transition temperature (T_c). Although monolayers generally provided superior optical performance, multilayers deposited at higher Ta target currents enabled more effective and reproducible control of the doping level. The best performance for monolayers was achieved with 0.9 at.% Ta, yielding a T_c of 49.9 °C at heating, a luminous transmittance (T_{lum}) near 50%, and solar modulation (ΔT_{sol}) and infrared solar modulation (ΔT_{IR}) capacities of 4.4% and 9.4%, respectively. For multilayers, the sample with 1.67 at.% Ta has T_c = 51 °C, T_{lum} = 47.3%, ΔT_{sol} = 4.3%, and ΔT_{IR} = 8.2%. With T_c values up to 16 °C lower than those of undoped films produced under comparable conditions, these results indicate that Ta doping presents a promising alternative to existing dopants, enabling significant T_c reduction without substantially compromising the properties required for VO_2-based smart-window applications.

1. Introduction

Improving energy efficiency and reducing CO_2 emissions have become key strategies for addressing climate change concerns [1,2]. Currently, building energy consumption accounts for more than 40% of global energy demand [3–5] and more than 50% of that energy goes to cooling, heating and indoor lighting [1,3–5]. Windows are the most vulnerable parts of the building with respect to heat gain and loss [6], thus being considered the least energy efficient component of the building [1,4,7]. This is why the development of smart windows, capable of dynamically controlling the transmission of solar radiation, is considered an effective means to reduce energy consumption [4,8]. Specifically, energy savings associated with the use of smart windows are estimated to be between 40 and 50% [8,9]. In this sense, although there are different types of smart windows, thermochromic glasses are assumed as the most suitable, since they are able to passively block IR radiation depending on the outside temperature without additional energy input [4].

Vanadium dioxide, VO_2, is the most studied thermochromic material [10], since it presents a reversible transition at a relatively low temperature of 68 °C [10–13]. This transition, known as metal-to-insulator (MIT), is accompanied by a structural phase transformation (SPT), which implies a change in the electrical, thermal and optical properties of the material as a function of temperature [14–17]. When the temperature increases until reaching the critical value, VO_2(M) is transformed into VO_2(R), i.e., the transformation from a monoclinic phase,

* Corresponding author at: IMEYMAT: Institute of Research on Electron Microscopy and Materials of the University of Cádiz, E-11510 Puerto Real, Spain.
E-mail address: antonio.santos@uca.es (A.J. Santos).

https://doi.org/10.1016/j.apsusc.2026.166230
Received 24 November 2025; Received in revised form 27 January 2026; Accepted 5 February 2026
Available online 8 February 2026
0169-4332/© 2026 The Author(s). Published by Elsevier B.V. This is an open access article under the CC BY-NC-ND license (http://creativecommons.org/licenses/by-nc-nd/4.0/).

transparent to IR radiation, to a rutile phase that mainly reflects this radiation [10,11,13,18]. However, in its pure form, this compound exhibits low luminous transmittance and poor solar modulation efficiency [18–22] with values typically around 40% and 10%, respectively [19,21]. This, coupled with a transition temperature (T_c) not low enough (hot is felt between 25 and 40 °C), hinders its potential to be an ideal material for smart windows applications [18–22].

Nowadays, research is focusing on two main strategies: Improving luminous transmittance and solar modulation capacity through structure engineering and reducing the phase transition temperature by doping [21]. It has been observed that T_c can be reduced by doping with high-valence cations, including W^{6+}, Mo^{6+}, Nb^{5+}, and Ta^{5+}. On the contrary, it increases by doping with low-valence cations such as Ti^{2+}, Ga^{3+}, and Cr^{3+} [22,23]. Among the different dopants, tungsten is considered the most effective in reducing T_c, with a decrease of 20-26 °C per atomic percentage [24–26]; however, W doping often results in a degradation of both T_{lum} and ΔT_{sol} [27,28], thus making it difficult to be applied in smart windows [24]. Ta doping, although less effective than W in reducing T_c, has been reported to enhance T_{lum} without a significant loss of ΔT_{sol} and is thus considered a promising alternative dopant for thermochromic VO_2-based coatings [24,28].

The reduction of the transition temperature in Ta-doped VO_2 stems from the synergistic interplay between electronic and structural effects. High-valence Ta^{5+} substitution for V^{4+} induces partial electron transfer into the V 3d states, creating V^{3+}-Ta^{5+} and V^{3+}-V^{4+} configurations that destabilize the semiconducting phase and consequently lower T_c [24]. Simultaneously, the larger ionic radius of Ta^{5+} compared to V^{4+} induces local lattice expansion and strain, which lowers the energetic barrier between the monoclinic and rutile phases. These two mechanisms are widely reported to act cooperatively in Ta-doped VO_2 systems [24,28,29].

Various techniques have been employed for the synthesis of VO_2 thin films, such as magnetron sputtering, chemical vapor deposition, pulsed laser deposition, electron beam deposition, hydrothermal, and sol–gel synthesis, among others [10,30], Magnetron sputtering has received considerable attention due to the possibility of depositing large areas [31,32] at low temperature [23,31], its compatibility with a wide range of substrates, and its environmental friendliness [23]. Also, doping with chemical elements is easy to achieve during this process [33]. In this context, the research of our group have revealed that, thanks to the exhaustive control of the deposition and annealing parameters, the fabrication of highly efficient VO_2-based films on glass substrates can be achieved by a simple two-step approach consisting of the rapid high-temperature oxidation of porous V or VO_x films obtained by the glancing angle deposition technique (GLAD) [34–36]. Likewise, these authors designed an alternative route for the synthesis of W-doped VO_2-based coatings by combining the co-deposition of $VO_y/V_{0.85}W_{0.15}O_y$ multilayers, thanks to which it is possible to control the doping percentage during the deposition [37].

Based on these recent studies, the present work focuses on the synthesis of Ta-doped VO_2 thin films on glass substrates. The deposition of these films involves, on the one hand, the simultaneous sputtering of vanadium and tantalum single layers and, on the other hand, the deposition of alternating $VO_y/V_{0.916}Ta_{0.084}O_y$ multilayers. Both configurations allow to control the overall coating composition either by adjusting the Ta target current or the thickness of the multilayers, respectively. The effect of different oxygen injection times (t_{ON}) used during deposition is also investigated. These coatings are then subjected to rapid thermal annealing in air atmosphere to synthesize and stabilize the thermochromic VO_2(M) phase. Eventually, the thermochromic behavior of films provided with different dopant ratios is examined by Vis-NIR spectrophotometry. The main objective is the study of an alternative dopant, different from W, which allows to obtain films with a more balanced optical performance. The analysis of the aforementioned variables allows, firstly, to examine how the deposition variants (monolayer and multilayer) as well as the effect of pulsed oxygen, affect the final optical behavior of the material and, secondly, to analyze the thermochromic behavior of samples with different amounts of dopant.

2. Materials and methods

2.1. Deposition process

Thin films were deposited at room temperature by direct current (DC) magnetron sputtering using two opposite metallic targets (51 mm of diameter and 99.9% purity): vanadium and tantalum. They were located inside a 40 L homemade vacuum chamber evacuated down to 10^{-5} Pa before each run by means of a turbomolecular pump backed by a primary pump. The distances between V and Ta target centers and the glass substrate (Menzel Gläser ® microscope slides) were fixed to 65 mm and 95 mm, respectively. On the basis of our previous studies [36], porous films with large surface-to-volume ratios and enhanced reactivity with oxygen were deposited by combining GLancing Angle Deposition (GLAD) and Reactive Gas Pulsing Process (RGPP) techniques. The deposition angles α (average angle of incoming particle flux) relative to the substrate normal were set at $\alpha = 85°$ and 75° for V and Ta, respectively, with no rotation of the substrate. Argon was injected at a mass flow rate of 2.40 sccm and the pumping speed was maintained at $S = 13.5$ L s^{-1}, whereas the oxygen gas was periodically supplied into the sputtering chamber. A rectangular pulsed signal was employed for the O_2 flow rate with respect to time evolution. The pulsing period was set at $P = 16$ s. The maximum oxygen flow rate was $q_{O2Max} = 0.40$ sccm. It corresponds to the critical flow required to trigger the process in the compound sputtering mode. The minimum flow rate was $q_{O2min} = 0$ sccm, while the oxygen injection time (t_{ON}) was set for times between 0 and 8 s. Based on these conditions, $V_xTa_{1-x}O_y$ films were obtained in monolayer and multilayer configurations of different compositions. For this purpose, a fixed current for the V target of 200 mA was used, while the current of the Ta was set at 5 mA (minimum current to generate a stable Ta plasma) for the monolayer deposition and at 20 mA for the multilayer.

2.2. Thermal treatments

After deposition, the samples were thermally treated in a lamp annealing system (MILA 5000 from ULVAC). The sample was placed on a transparent quartz support held through a tube of the same material, which was cooled with water. During the process, it was possible to insert an air flow, which can be measured by means of a rotameter. In this case, the samples were heat treated at a temperature of 510 °C for a period of 10 s, for which a heating ramp of 40 °C s^{-1} was used. Finally, all the samples were left to cool at room temperature inside the furnace. An air flow rate of 10 l min^{-1} was used throughout the process.

2.3. Compositional and functional characterizations

Topographic micrographs of the reference samples were acquired using a Thermo Scientific Scios 2 DualBeam analytical focused ion beam-scanning electron microscopy (FIB-SEM) system operating at 5 kV. This instrument was also used to prepare electron-transparent cross-section lamellae for (scanning)-transmission electron microscopy ((S) TEM) analyses. High-angle annular dark-field (HAADF) imaging and energy-dispersive X-ray spectroscopy (EDX) analyses were performed in a Thermo Fisher Scientific TALOS F200X analytical microscope working at an accelerating voltage of 200 kV and equipped with a Super-X detection system comprising four silicon drift detectors arranged around the sample. A Gatan Imaging Filter (GIF) Continuum system fitted to the Talos microscope was used for spatially resolved electron energy-loss spectroscopy (EELS) in scanning-transmission (STEM) mode. STEM-EELS 2D spectrum image (SI) datasets were acquired using a 2.5 mm diameter aperture and an energy dispersion 0.05 eV/channel. The camera length was 47 mm, yielding convergence and collection

semi-angles of 10.5 and 20.0 mrad, respectively, and the probe current was 150–175 pA depending on the experiment. To enable accurate chemical-shift measurements, the Dual EELS mode was employed to record nearly simultaneously both low-loss signal and the V-$L_{2,3}$ and O-K high-loss edges at each pixel position. A dwell time of approximately 0.2 s per pixel was selected to optimize the signal-to-noise ratio. The thermochromic behavior of prepared Ta-doped VO_2 films was determined via transmission spectroscopy using a PerkinElmer Lambda 900 UV/VIS/NIR Spectrometer equipped with a THMS600 Linkam stage for temperature control. UV–Vis-NIR transmittance spectra were recorded in the wavelength range of 300–2500 nm at selected temperatures in the range of 15–90 °C. For the dynamic monitoring of the thermally induced phase transition, the thermal evolution of the optical transmittance at a selected NIR wavelength (2000 nm) was recorded during consecutive heating–cooling cycles at a controlled heating rate of 5 °C min^{-1} and cooling rate of 2 °C min^{-1}.

3. Results and discussion

3.1. Compositions of reference samples

To determine the co-deposition conditions necessary to obtain the desired doping ratios, a total of four $V_xTa_{1-x}O_y$ reference samples with a nominal thickness of 300 nm were deposited. A constant target current was used: Two samples with currents applied to vanadium and tantalum targets of 200–5 mA, respectively, and two others with currents of 200–20 mA. Additionally, oxygen injection times of 0, 4, and 8 s were used. Analogous to a previous work [37], which showed that the W/V ratios of $V_xW_{1-x}O_y$ precursors are preserved in $V_xW_{1-x}O_2$ films after heat treatments, samples with (1-x)/x ratios will be referred to as (1-x) Ta in this case (e.g., Ta/V = 1/99 is referred to as 1Ta). This makes easier the aforementioned designation, comparison and interpretation of results [24,28,38].

Fig. 1 shows the (S)TEM-EDX studies carried out on a reference sample of 300 nm nominal thickness deposited with 200–20 mA currents and 8 s of oxygen pulse. The EDX analyses performed on this sample revealed that the introduction of oxygen does not significantly affect the deposited Ta ratio, yielding an average composition of 2.7Ta for the 200–5 mA currents and 8.4Ta for the 200–20 mA currents. The details of the process carried out to obtain these results can be found in the Supplementary Material. What is indeed observed in the integrated EDX spectrum is that, despite the fact that the spectra were acquired in V-rich and Ta-rich areas, signals belonging to different elements appear. The peaks corresponding to Na, Si, and Ca are due to the substrate. Mo is due to the support grid, while C corresponds to contamination derived from the handling, cleaning and probing of the sample.

A literature analysis indicates that the optimal Ta doping level lies between 2 and 4Ta, with an upper limit of 6Ta. Specifically, B. Li *et al.* [28] identifies 4Ta as the optimal doping, achieving a reduction in the critical temperature to approximately 25 °C. However, they noted that, for the solar modulation ability to remain constant, the doping should be below 3Ta. Consistent with this, Sun *et al.*'s work [38] suggests an optimal doping around 4.35Ta, with a T_c of about 30 °C. In contrast, Xu *et al.* [39] achieved the best results with a lower Ta/V atomic ratio, at a doping level of 0.71 at.% (approximately 2.1Ta). Finally, Chen *et al.*'s study [24] revealed that the critical Ta content beyond which the optical behavior of the films deteriorates is 6.3Ta.

Our results indicate that while a 2.7Ta composition falls within the optimal range for Ta doping of these coatings, it remains necessary to analyze the impact of varying proportions of this dopant on their optical properties. To achieve this, a complementary strategy based on the deposition of alternating multilayers of $VO_y/V_{0.916}Ta_{0.084}O_y$, which allows to reach desired average dopant amounts, was adopted. For this purpose, the tantalum deposition times were determined and controlled by opening and closing its associated target shutter, allowing concentrations below 8.4Ta (excessive dopant concentration according to the literature). To obtain highly reproducible films, we followed these rules: (1) the minimum Ta deposition time in each individual layer could not be less than 5 s to avoid artifacts caused by shutter movement; (2) depending on the conditions, the largest possible number of sublayers of $V_{0.916}Ta_{0.084}O_y$ would be deposited to favor greater diffusion of the dopant element, thus obtaining films whose behavior is analogous to a film deposited by monolayer.

Once the optimal co-deposition conditions were established, thin films of $V_{0.973}Ta_{0.027}O_y$, deposited as monolayers, and multilayers of $VO_y/V_{0.916}Ta_{0.084}Oy$, with a nominal thickness of 50 nm and compositions of 1Ta, 2.7Ta, 3Ta, and 5Ta, were fabricated. All samples addressed in this study, along with their deposition conditions, are listed in Table 1. Each sample was then subjected to a rapid thermal annealing (RTA) at 510 °C during 10 s to obtain $V_xTa_{1-x}O_2$-based thermochromic coatings. These annealing conditions were selected based on previous studies on VO_x-derived films [34,36], which have shown that short treatments are sufficient to achieve complete oxidation and crystallization for comparable layer thicknesses. Compared to conventional

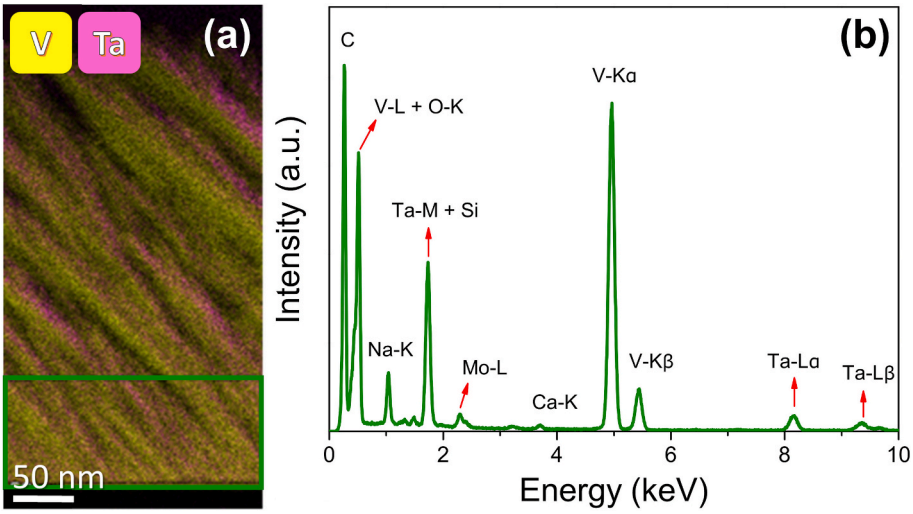


Fig. 1. Scanning-transmission electron microscopy analysis performed on a nominally 300 nm thick $V_xTa_{1-x}O_y$ film, deposited with vanadium and tantalum target currents of 200 and 20 mA, respectively. (a) STEM-EDX net intensity maps obtained for V and Ta atoms. (b) EDX integrated spectra for the region defined by a green square in (a).

Table 1
Deposition conditions for $V_xTa_{1-x}O_y$ samples of 50 nm nominal layer thickness. t_{ON} is the oxygen injection time.

Sample	Ta doping (at.%) in $V_xTa_{1-x}O_y$	Number of $V_{0.916}Ta_{0.084}O_y$ multilayers	t_{ON} (s)
1Ta_8	0.33	16	8
2.7Ta_0	0.90	–	0
2.7Ta_4			4
2.7Ta_8			8
3Ta_0	1.00	16	0
3Ta_4			4
3Ta_8			8
5Ta_8	1.67	16	8

long-duration annealing, RTA reduces the thermal budget and limits alkali diffusion from glass substrates, leading to polycrystalline microstructures that typically exhibit relatively broad hysteresis loops and, in some cases, beneficial reductions of the metal–insulator transition temperature.

3.2. Compositional features of annealed samples

Before presenting other results, Fig. 2 provides an overview of the structure obtained of sample 3Ta_8 after thermal treatment. The low-magnification STEM-HAADF micrograph reveals a grain-like morphology and an average film thickness between 60 and 70 nm, according to the available measurements.

In order to confirm the main nature of the resulting layers after the thermal treatments, EELS analyses were carried out. Fig. 3 summarizes the most representative findings. Fig. 3(a) is an HAADF micrograph where both the substrate and the VO_2-based film can be distinguished. This region of the film was scanned with the STEM probe under specific conditions in order to retrieve EELS spectra which would allow to identify the resulting vanadium oxides after annealing. Fig. 3(b) is a compilation of the main EELS spectra obtained throughout regions like the ones marked in Fig. 3(a). All four spectra display the same characteristic features, confirming that the same vanadium oxide is present throughout these regions.

Specifically, four distinct energy-loss features appear at comparable energy ranges: the L3 and L2 vanadium white lines (at about 516.3 eV and 522.8 eV, respectively) and the t_{2g} and e_g oxygen pre-edge (at about 518.2 eV and 530.5 eV, respectively). In addition, both V white lines exhibit small low-energy shoulders, also consistently observed across spectra. These elements closely match the fingerprints reported in previous studies [40,41] for vanadium dioxide (VO_2), supporting that the applied thermal treatment successfully produces VO_2 in the Ta-doped layers.

3.3. Analysis of samples with different arrangement and composition

3.3.1. Influence of sample architecture on the optical behavior

To determine and characterize the thermochromic effect, the transmittance spectra of the fabricated samples were recorded in the 300–2500 nm range at 15 °C and 90 °C, i.e., below and above the critical temperature of VO_2 (Fig. 4).

The spectra shown correspond to samples of similar Ta content (2.7Ta and 3Ta) deposited using monolayers and multilayers, respectively. As mentioned in the first section, the aim is to determine the differences observed according to the type of deposition and to evaluate how the injection of an oxygen pulse during deposition affects the thermochromic properties.

At low temperature, it is worth noticing that the transmittance of the samples increases sharply upon reaching the visible range after UV absorption and then decreases to a minimum above 1000 nm, at which point it begins to increase to transmittances of 50–70% at 2500 nm. However, when the temperature of the samples is 90 °C, the transmittance decreases from 750 nm, the beginning of the infrared radiation range, which is characteristic of the thermochromic behavior of material, thus demonstrating the formation of vanadium dioxide.

In particular, the samples deposited without oxygen injection (t_{ON} = 0 s) show a slightly higher transmittance in the visible range than the samples with t_{ON} = 4 s. This observation does not apply to the samples with t_{ON} = 8 s, as it is only valid for the sample deposited in multilayers. Furthermore, the transmittance in the near-infrared (NIR) is similar for all samples, with the exception of the sample with t_{ON} = 8 s deposited in a monolayer and the sample with t_{ON} = 4 s deposited in a multilayer. These exceptions exhibit transmittances, implying lower radiation absorption, which would be detrimental for their application compared to other samples.

Thermochromic parameters, including luminous transmittance (T_{lum}), solar modulation (ΔT_{sol}), and solar infrared modulation (ΔT_{IR}), which were determined from the above spectra, are shown in Table 2. These parameters allow a quantitative comparison of the samples and, therefore, their potential applicability in smart windows. The definition and detailed explanation of the calculation of all these parameters can be found in the work of Outón *et al.* (Appendix A) [42].

As expected from the spectra, the luminous transmittances are relatively positive, between 40 and 50%, especially considering the thickness of these samples as well as the doping level [43,44]. At this stage, it can be seen that, for the monolayers, the highest luminous transmittance corresponds to the sample with t_{ON} = 8 s, being lower but similar for the samples with t_{ON} = 0 and 4 s. Conversely, the highest value associated with the multilayers corresponds to the sample deposited with t_{ON} = 0 s, this being significantly higher than that of the samples with t_{ON} = 4 and

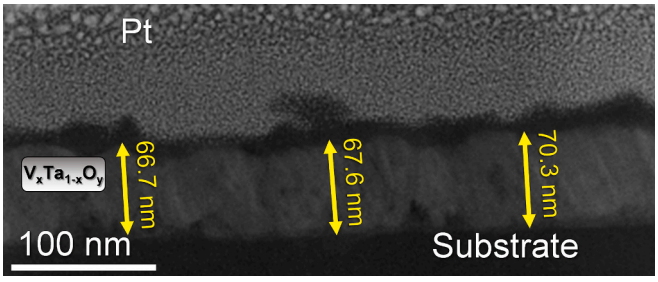


Fig. 2. Low-magnification STEM-HAADF micrograph of sample 3Ta_8 indicating some exemplary thickness measurements of the resulting film.

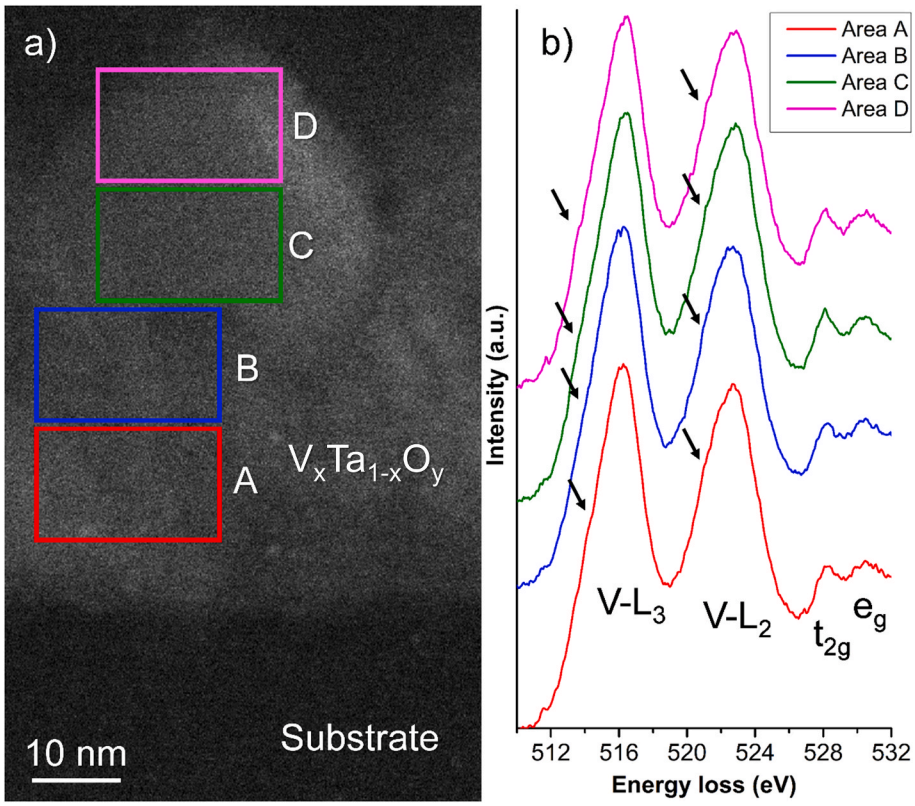


Fig. 3. STEM-HAADF micrograph of sample 3Ta_8 showing areas where EELS spectra were gathered (a) and resulting EELS spectra indicating the main features of $V_xTa_{1-x}O_y$ compounds (b).

8 s. Regarding solar modulation capacity, moderate values are obtained in all cases, these being higher for solar infrared modulation and higher for the samples with t_{ON} = 0 s. Having analyzed these parameters, it appears that the deposited samples, both in monolayers and multilayers, with oxygen injection times of 0 s, are the optimal ones for this study. Finally, it has been shown that the coexistence of VO_2(M) and V_2O_5 phases usually leads to high ΔT_{lum} values [34], which positively impacts the solar modulation ability of the films. This would explain why the 2.7Ta_0 and 3Ta_0 samples exhibit the highest ΔT_{lum} and ΔT_{sol} values.

For a more in-depth analysis, experiments on the kinetics of the transmittance evolution of the samples at 2000 nm during heating and cooling cycles are examined (Fig. 5). It is observed that the transmittance decreases as the temperature increases until it reaches T_c, which indicates that the transformation from the monoclinic phase, VO_2(M), to the rutile phase, VO_2(R), is taking place. Moreover, when the temperature decreases, the transmittance recovers its initial values, describing the typical hysteresis cycle common to all physical properties of this type of material (Fig. 5(a–b)).

The behavior described is common to all the samples, although we can observe that as t_{ON} increases, the hysteresis cycles shift to the left, which indicates that the transition temperatures, both in the heating and cooling branches, decrease. This implies that, for the same Ta content, as the oxygen injection time increases, the critical temperature of the samples decreases, while the total transmittance drop seems to be unaffected, remaining in the range of 30–35% in all cases.

For a more precise analysis of the characteristic parameters of the kinetic curves, the respective derivative curves have been obtained, both during heating and cooling (Fig. 5(c–d). The parameter values associated with these curves are shown in Table 3. This shift of the hysteresis loops towards lower transition temperatures with increasing oxygen injection time is reflected in the respective derivative curves. A decrease in T_c, associated with the displacement of the minimum and maximum of the curves corresponding to the heating and cooling of the samples, respectively, is observed. It is also observed that, for the samples deposited in monolayers, this displacement is more gradual than in the case of multilayers, where the curves for the samples with t_{ON} 0 s and 4 s are similar.

The samples with t_{ON} 0 s exhibit higher critical temperatures, as shown in the previous curves, both during heating and cooling, being close to the typical T_c of pure VO_2 (68 °C), especially for the sample deposited in a monolayer (2.7Ta_0). One can notice a greater decrease in T_c for the samples deposited in monolayers, both for the heating and cooling branches. However, assuming the average of these values, the trend is even clearer in both cases. Taking into account the T_c value of pure VO_2, we can state that a decrease of up to 18 °C has been achieved if we consider the T_c of heating, which is the temperature typically used as a reference, and even up to 21 °C if considered the obtained average.

Finally, it is observed relatively broad hysteresis widths. For monolayer deposited samples, it is found a clear trend: As the oxygen injection time increases, the hysteresis width becomes narrow. Conversely, for multilayer deposited samples, no clear trend was apparent, with the largest width corresponding to the t_{ON} = 4 s sample. As reported in the literature, the hysteresis width of Ta-doped samples is smaller, decreasing in all cases as the Ta content increases, which could stem from different deposition conditions.

As a result, we can say that the synthesis of these films via monolayers or multilayers, and adjusting the Ta current for getting the same dopant content, leads to films with good optical performance, especially for a monolayered structure. The difference between the two configurations, considering that the Ta content is similar, could be due to the Ta diffusion in the single layers compared to the multilayers, where some Ta (either metallic or Ta^{5+}) might remain unincorporated into the VO_2 structure.

On the other hand, increasing t_{ON} affects the optical performance of the samples to some extent. The solar infrared modulation capacity is greater for those samples deposited with t_{ON} = 0 s, in both

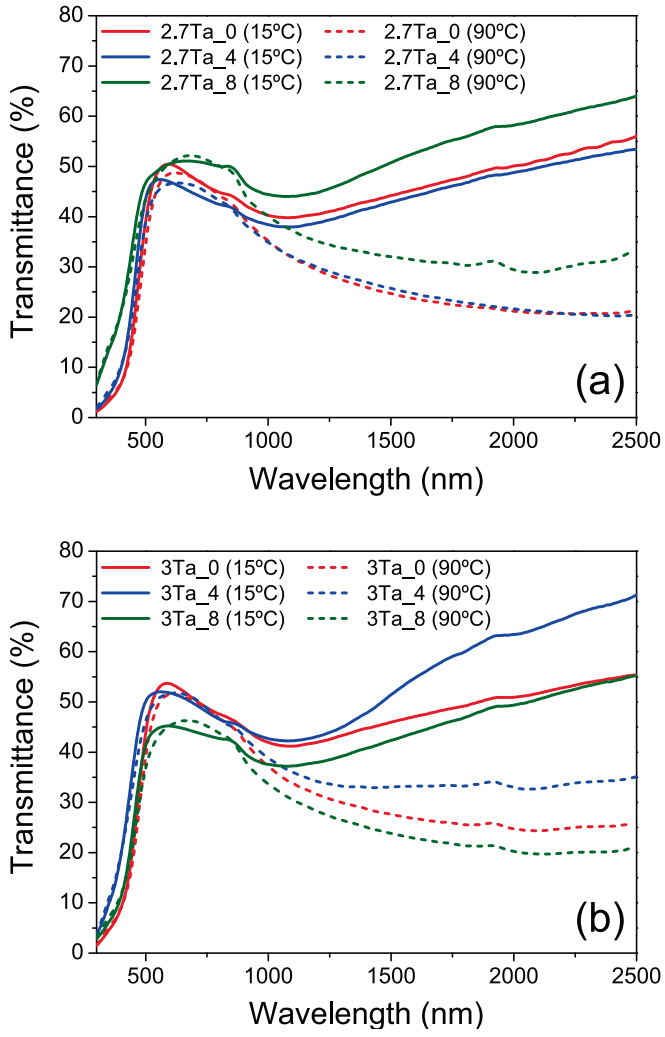


Fig. 4. UV–Vis-NIR transmittance measurements performed at low (15 °C) and high (90 °C) temperatures on samples deposited in monolayers (a) and multilayers (b).

Table 2
Photometric (T_{lum}) and radiometric (T_{sol}, T_{IR}) parameters and their variation with temperature, Ta concentration and t_{ON} time. The accuracy of these values is ±0.1%.

Sample	$T_{lum,avg.}$ (%)	ΔT_{lum} (%)	ΔT_{sol} (%)	ΔT_{IR} (%)
2.7Ta_0	45.6	2.8	5.3	10.2
2.7Ta_4	45.0	2.0	4.1	8.5
2.7Ta_8	48.4	1.0	4.4	9.4
3Ta_0	49.2	3.0	5.2	9.5
3Ta_4	43.4	0.7	3.8	8.7
3Ta_8	43.1	1.5	4.2	9.1

configurations, while the luminous transmittance decreases with increasing t_{ON} for multilayers and increases for monolayers. At the same time, longer injection times lead to a systematic reduction of the critical temperature. This behavior can be rationalized considering that, in GLAD deposited VO_x thin films with nominal thicknesses below ~ 50 nm, higher t_{ON} values are associated with increased oxygen incorporation and a growth regime increasingly governed by diffusion processes, resulting in more homogeneous microstructures and modified local stoichiometry [36,40]. In Ta-doped VO_2, such conditions can reinforce lattice distortions associated with Ta^{5+} substitution for V^{4+}, as reported in the literature [45]. The combined effect of increased oxygen content and Ta-induced lattice strain provides a physically consistent explanation for the observed decrease in T_c.

Accordingly, samples deposited with 8 s of oxygen injection were selected for further analysis, as they offer a favorable balance between reduced transition temperature and preserved optical performance in both monolayer and multilayer configurations.

Fig. 6 presents the SEM micrographs of the 2.7Ta_8 and 3Ta_8 samples to analyze, in depth, the variation of the thermochromic parameters of the samples with ton 8 s. The objective is to verify whether the surface morphology of these samples is affected by the deposition configuration and how this might affect their optical performance. Fig. 6 (a) shows a surface characterized by a small grain size and high porosity, whereas Fig. 6(b), corresponding to the 3Ta_8 sample, exhibits a markedly different morphology, consisting of large elongated grains with a rod-like appearance, commonly associated with V_2O_5 [46,47]. However, it is important to clarify that these microstructural features are confined to the near-surface region and do not necessarily reflect the composition of the bulk of the film. If the coating were predominantly composed of V_2O_5, the thermochromic response observed in all samples would not be possible. Instead, the clear thermochromic behavior, in good agreement with the STEM-EELS analyses, indicates that the dominant phase throughout the film thickness is $V_xTa_{1-x}O_2$.

Therefore, the distinct morphology observed in sample 3Ta_8 may be associated with surface-related effects, likely arising from localized oxidation of the near-surface region, rather than from a change in the bulk phase. Nevertheless, the pronounced grain growth and reduced porosity of this surface layer result in a rough and inhomogeneous morphology, which can enhance light scattering and thus contribute to the significantly lower luminous transmittance measured for this sample (43.8%).

3.3.2. *Variation of the Ta/V ratio and its effect on the optical behavior*

In the previous section, it was demonstrated that the samples deposited as monolayers offered better results with respect to their optical behavior. Nevertheless, the adoption of this monolayer configuration presents a distinct limitation in terms of compositional adjustability. In fact, working with currents below 5 mA can result in plasma instability, leading to conditions lacking in reproducibility. Employing a current of 20 mA enables greater control over the composition, thereby allowing us to examine the correlation between varying dopant concentrations and optical properties. Therefore, to focus on the study of Ta doping, a current of 20 mA will be used for the dopant target. Selecting samples with oxygen injection times of 8 s and Ta contents of 1Ta, 3Ta, and 5Ta will be done. This involves including two additional samples with lower and higher Ta concentrations, respectively.

Representative SEM micrographs of the investigated films are shown in Fig. 7. Samples 1Ta_8 and 5Ta_8 exhibit generally compact grains with relatively uniform shapes. Sample 5Ta_8 appears to have slightly larger grains than 1Ta_8, which may qualitatively relate to a minor reduction in luminous transmittance. Generally, an increase in dopant concentration is expected to result in a reduction in grain size [33]; however, for the selected Ta/V ratios in this study, this trend is not observed. In contrast, the 3Ta_8 sample displays a markedly different surface morphology, characterized by large, elongated grains with a rod-like appearance, previously noted as an exceptional surface feature reminiscent of V_2O_5. Due to this distinctive surface structure, it is also expected that 3Ta_8 exhibits lower luminous transmittance compared to the other two samples.

Following the SEM analysis, the optical behavior of the films was examined through UV–Vis-NIR spectroscopy. The transmittance spectra of the three samples are presented in Fig. 8, providing an overview of their optical response across the visible and near −infrared regions. It can be observed that the samples with Ta contents of 1Ta_8 and 5Ta_8 present similar transmittances in the visible range, with the exception of

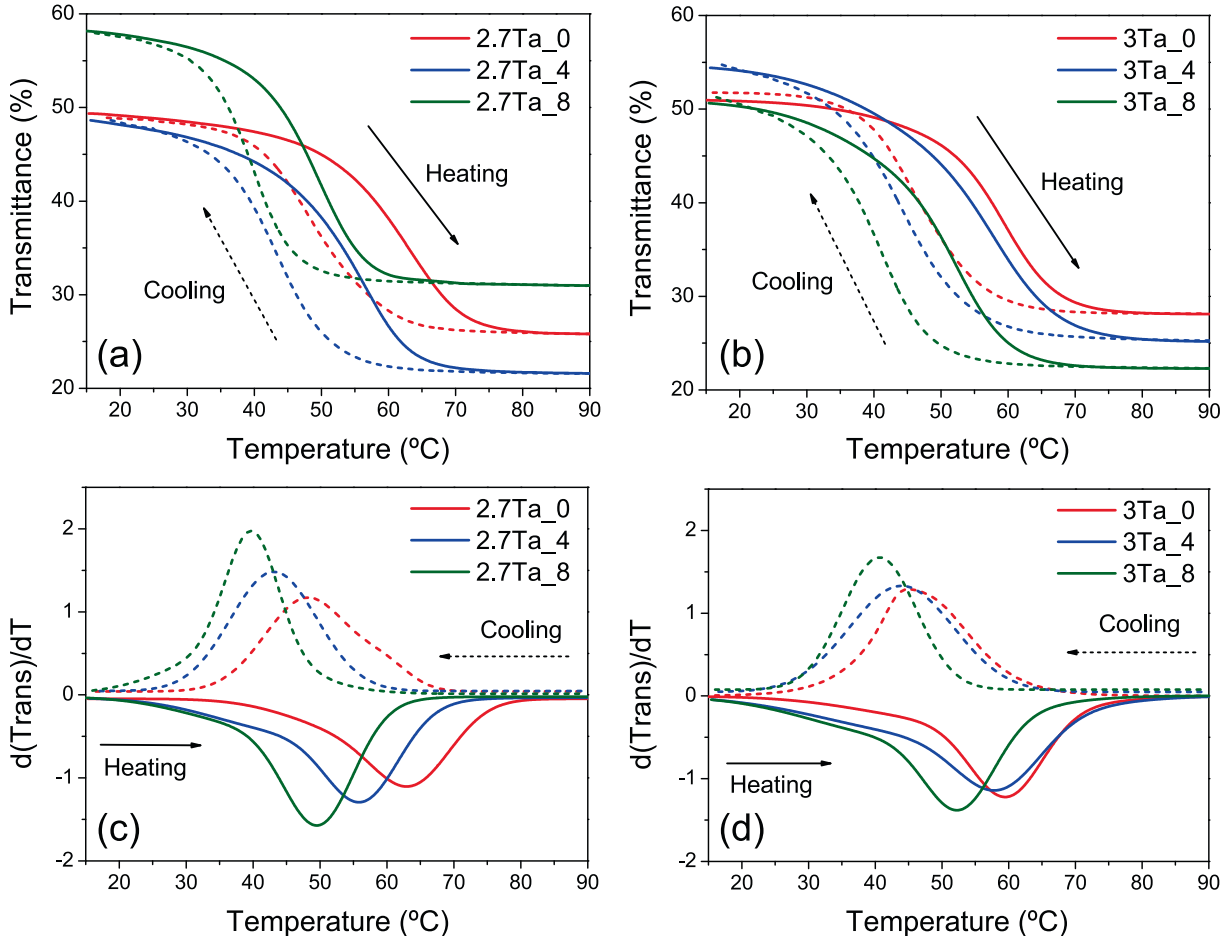


Fig. 5. (a and b) Kinetics of the evolution of the infrared transmittance at 2000 nm of samples subjected to consecutive heating and cooling cycles. (c and d) Derivative curves from the infrared transmittance kinetics as a function of temperature. For a better overview, the cooling derivatives are represented in absolute values.

Table 3
Values obtained from the differential analysis of the kinetic curves of the transmittance evolution as a function of temperature. $T_{c,h}$ and $T_{c,c}$ indicate the MIT transition temperature on heating and cooling, respectively. $T_{c,avg.}$ is defined as the average of $T_{c,h}$ and $T_{c,c}$. W_H is the hysteresis width and is given by the difference between $T_{c,h}$ and $T_{c,c}$. The accuracy of temperature and transmittance values are ±0.5 °C and ±0.1%, respectively.

Sample	$T_{c,h}$ (°C)	$T_{c,c}$ (°C)	$T_{c,avg.}$ (°C)	W_H (°C)
2.7Ta_0	63.9	48.2	56.1	15.7
2.7Ta_4	56.4	43.1	49.8	13.3
2.7Ta_8	49.9	39.8	44.9	10.1
3Ta_0	59.8	47.5	53.7	12.3
3Ta_4	58.6	43.9	51.3	14.7
3Ta_8	52.7	40.6	46.7	12.1

the 3Ta_8 sample, which is noticeably lower. Regarding NIR transmittances, samples 3Ta_8 and 5Ta_8 show quite similar behavior, while sample 1Ta_8 exhibit higher transmittance at both low and high temperatures. In any case, the reported NIR transmittance drops are equivalent for all these samples, which does not denote, at least preliminarily, a progressive deterioration of the solar modulation ability as the dopant concentration increases.

Table 4 shows the thermochromic parameters determined from the spectra shown in Fig. 8. As can be seen, the luminous transmittance obtained is quite worthy for the 1Ta_8 and 5Ta_8 samples, being close to 50%, while the 3Ta_8 sample presents a somewhat lower value (T_{lum} = 43.1%), consistent with the distinct surface morphology observed in its SEM micrographs. With respect to the solar modulation, moderate values (ΔT_{sol} = 4.2–4.3%) are obtained in all cases, which confirms that the increase in dopant concentration, at least within the chosen concentrations, does not significantly affect the solar modulation. Finally, with respect to the infrared modulation, we observe that the values are slightly higher, as expected, with the highest value obtained for the 3Ta_8 sample. On the other hand, according to the literature [28], the solar modulation remains almost constant with increasing dopant concentration, although, in this case, so does the solar infrared modulation.

For further analysis, experiments on the kinetics of transmittance evolution at 2000 nm were performed as the samples were subjected to consecutive heating and cooling cycles (Fig. 9). According to Fig. 9(a), the samples again exhibit the typical hysteresis loop, although this time with one key difference: As the Ta content increases, the transmittance at 2000 nm decreases. This observation would initially suggest a decrease in ΔT_{sol}. However, we note that the solar modulation ability remains nearly constant, which could be attributed to the ΔT_{lum}, with its

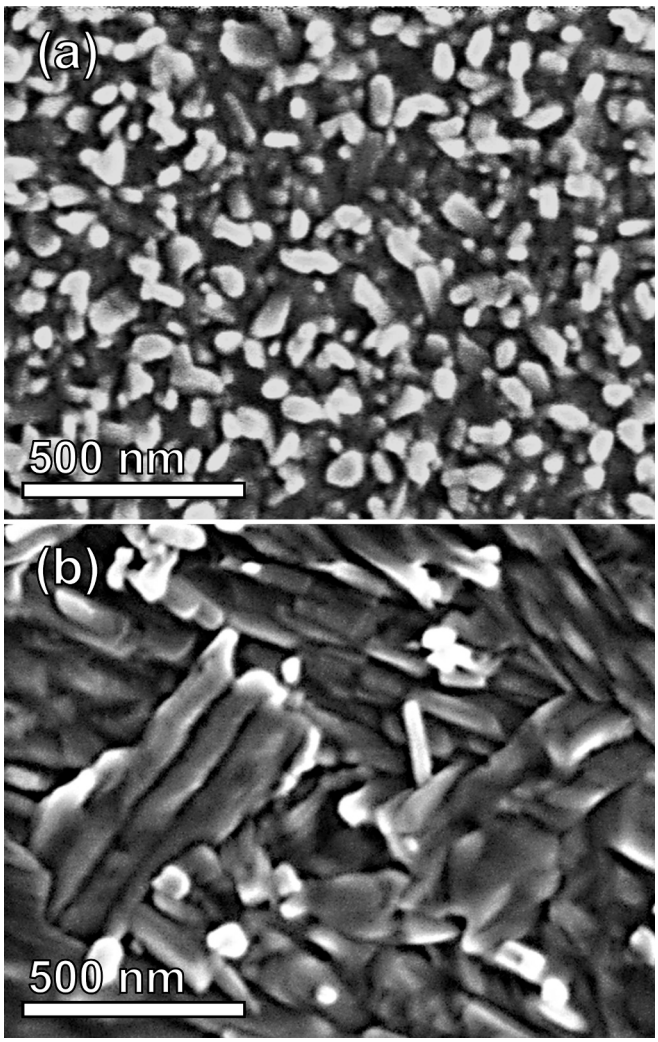


Fig. 6. SEM micrographs of the surface morphology of samples (a) 2.7Ta_8, (b) 3Ta_8.

highest value observed for the 5Ta_8 sample. Likewise, this shift towards lower transmittances is not the only change: It is also evidenced a shift of these hysteresis loops toward lower temperatures. This implies that the transformation from the monoclinic phase to the rutile phase occurs at lower T_c when increasing Ta concentration, indicating an effective doping.

For a more precise analysis of the characteristic parameters of the kinetics curves, the respective derivative curves were obtained for both heating and cooling cycles (Fig. 9(b)). The progressive shift of the hysteresis loops towards lower temperatures with increasing doping concentration is again reflected in the respective derivative curves. A decrease in T_c associated with this shift is observed, especially in the heating branch, where the positions of the minimum of the curves are shifted slightly to the left. Surprisingly, the T_c temperatures for the cooling branch, where the position of the maximum peaks is always located, remain practically unchanged, eventually resulting in narrower hysteresis as Ta doping increases, in fine agreement with the study by Xue *et al.* [33].

Additionally, it is also observed that the absolute values of the maxima and minima decrease with increasing Ta content, suggesting a more gradual transition that enhances comfort. Notably, increasing the Ta/V ratio in our samples yields a smoother transformation, and this, together with the lowered T_c, highlights the value of our results. Table 5 compiles the values of T_c for both heating and cooling, the average T_c, and W_H, as determined by differential analysis. It should be noted that, when referenced against previous studies involving undoped samples

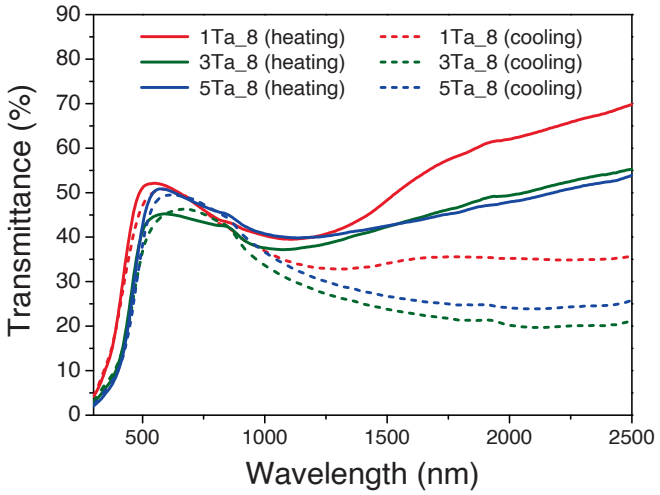


Fig. 8. UV–Vis-NIR transmittance spectra measured in the range 300–2500 nm for different Ta contents, at 15 °C and 90 °C.

Table 4
Luminous transmittance and solar and infrared modulation capacity values for the different samples. The accuracy of these values is ±0.1%.

Sample	T_{lum} (%)		T_{sol} (%)	T_{IR} (%)
	$T_{lum,avg.}$	ΔT_{lum}	ΔT_{sol}	ΔT_{IR}
1Ta_8	50.4	1.8	4.2	8.0
3Ta_8	43.1	1.5	4.2	9.1
5Ta_8	47.3	2.4	4.3	8.2

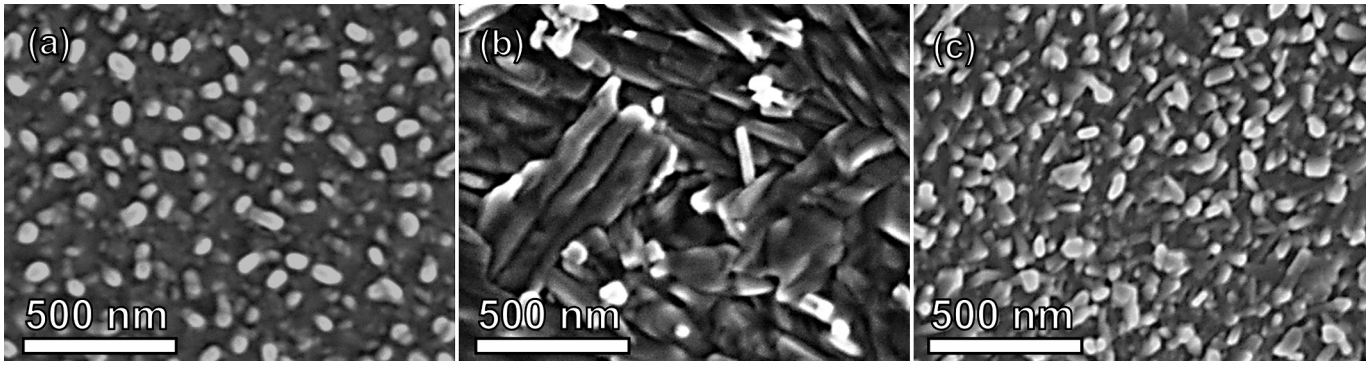


Fig. 7. SEM micrographs of the surface morphology of samples (a) 1Ta_8, (b) 3Ta_8 and (c) 5Ta_8.

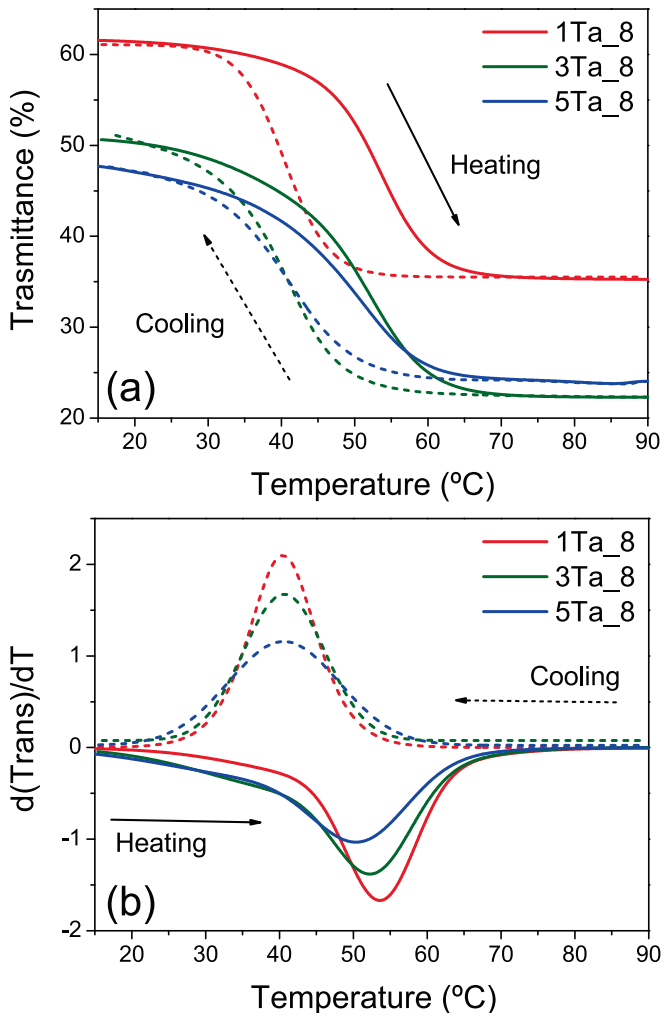


Fig. 9. (a) Kinetics of transmittance evolution at 2000 nm when the samples are subjected to consecutive heating (solid lines) and cooling (dashed dot lines) cycles. (b) Differential analysis of the transmittance kinetics curves versus temperature. For a better overview, the cooling derivatives are represented in absolute values.

Table 5
Critical temperatures and hysteresis widths obtained from the differential analysis of the kinetic curves of transmittance evolution as a function of temperature. The accuracy of temperature and transmittance values are ±0.5 °C and ±0.1%, respectively.

Sample	$T_{c,h}$ (°C)	$T_{c,c}$ (°C)	$T_{c,avg.}$ (°C)	W_H (°C)
1Ta_8	53.9	40.3	47.1	13.6
3Ta_8	52.7	40.6	46.7	12.1
5Ta_8	51.0	40.6	45.8	10.4

[36], Ta doping induces a $T_{c,h}$ reduction of up to 16 °C relative to comparable undoped films fabricated through similar procedures and layer thicknesses (62–66 °C). However, when compared with the optimal W-doped VO_2 films previously reported [37], which exhibit transition temperatures of 43–44 °C along with slightly higher luminous transmittance and comparable solar modulation performance, the T_c values achieved here (down to 51 °C) are more modest, despite the overall similar optical behavior.

Overall, these results demonstrate that Ta is effective in reducing the transition temperature of VO_2(M). Notably, the decrease in T_c is higher than expected (>8 °C per at.%), in line with the observations reported by Li *et al.* [28]. This effect is evident in the kinetic curves of the transmittance evolution at 2000 nm, where the hysteresis cycles shifted towards lower temperatures as the amount of Ta increased. Similarly, this increase in dopant concentration results in a reduction of the hysteresis width, whose behavior versus temperature is slightly different.

4. Conclusions

$V_xTa_{1-x}O_2$ thin films were successfully fabricated, enabling a systemic evaluation of the effect of Ta incorporation on the optical properties of VO_2. Monolayer films exhibited overall superior optical performance, while multilayer architectures allowed flexible control of Ta concentration by using purely metallic targets.

Increasing the oxygen injection led to a systematic reduction of the phase transition temperature. The thermochromic behavior of the samples showed that higher Ta contents decrease T_c without significantly compromising luminous transmittance, solar modulation capacity, or infrared solar modulation capacity, while slightly narrowing the hysteresis, a desirable feature for switching applications.

The best-performing films achieved T_c values around 50 °C, representing a reduction of up to 16 °C compared to undoped VO_2, while maintaining T_{lum} values close to 50% and moderate modulation capacities. Although W typically induces a larger T_c decrease, Ta-doped films preserve optical properties close to those of undoped VO_2, highlighting Ta as a promising alternative dopant for tuning the thermochromic response of VO_2-based in smart-window applications.

CRediT authorship contribution statement

A. Casas-Acuña: Writing – review & editing, Writing – original draft, Visualization, Methodology, Investigation, Formal analysis, Conceptualization. **A.J. Santos:** Writing – review & editing, Writing – original draft, Visualization, Validation, Supervision, Project administration, Methodology, Conceptualization. **N. Martin:** Writing – review & editing, Supervision, Resources, Methodology, Funding acquisition, Conceptualization. **J.J. Jiménez:** Visualization, Methodology, Investigation, Formal analysis. **M. Garzón:** Methodology, Investigation. **R. García:** Writing – review & editing, Validation, Supervision, Resources. **F.M. Morales:** Writing – review & editing, Validation, Supervision, Resources, Project administration, Methodology, Funding acquisition, Conceptualization.

Declaration of competing interest

The authors declare that they have no known competing financial interests or personal relationships that could have appeared to influence the work reported in this paper.

Acknowledgements

A. Casas-Acuña would like to thank University of Cadiz for its support through the UCA/REC49VPCT/2022 fellowship and acknowledges funding from the Plan Propio (Ref. EST2023-128 and EST2024-124) for two stays at the FEMTO-ST Institute. A. J. Santos would like to thank to Junta de Andalucía/CUII and ESF+ program for the concession of a postdoctoral fellowship (2024-087/PAI/EIDIA DOC/CD). ELECMI-ICTS of the UCA R&D Central Services (SC-ICYT) is acknowledged by easing the access to electron microscopy mutual facilities. This work was supported by the Spanish State R&D project (Generación de Conocimiento) with reference PID2023-150975OB-I00. The "Plan Propio UCA 2025-2027" has also supported this work.

Appendix A. Supplementary data

Supplementary data to this article can be found online at https://doi.org/10.1016/j.apsusc.2026.166230.

Data availability

Data will be made available on request.

References

[1] K. Sun, Y. Xie, J. Chu, X. Zhang, Q. Lai, J. Qiu, J. Tan, Effect of VO_2 particle aggregation on the performance of thermochromic smart window films for building, Infrared Phys. Technol. 145 (2025) 105717, https://doi.org/10.1016/j.infrared.2025.105717.

[2] Y. Wang, X. Xu, Z. Hua, T. Zheng, Study on low-cost near-infrared smart window on general glass by simple method, Results Opt. 8 (2022) 100229, https://doi.org/10.1016/j.rio.2022.100229.

[3] Y. Qiao, Z. Tang, Z. Wu, J. Wang, X. Sun, F. Yu, C. Wang, J. Mao, Q. Zhang, F. Cao, VO_2-based colorful smart windows with self-cleaning function, Sol. Energy Mater. Sol. Cells 274 (2024) 113004, https://doi.org/10.1016/j.solmat.2024.113004.

[4] L. Hu, H. Zhu, K. Lu, C. Wang, L. Liu, L. Ma, Theoretical investigation of VO_2 smart window with large-scale dynamic infrared emittance adjustment for adaptive thermal management, Sol. Energy 277 (2024) 112734, https://doi.org/10.1016/j.solener.2024.112734.

[5] B. Wang, T. Wang, X. Wu, K. Yu, Adaptive photothermal management of smart window based on VO_2, Appl. Therm. Eng. 263 (2025) 125389, https://doi.org/10.1016/j.applthermaleng.2024.125389.

[6] S. Wang, T. Jiang, Y. Meng, R. Yang, G. Tan, Y. Long, Scalable thermochromic smart windows with passive radiative cooling regulation, Science 374 (2021) 1501–1504, https://doi.org/10.1126/science.abg029.

[7] C. Wen, L. Feng, Z. Li, J. Bai, S. Wang, X. Gao, J. Wang, W. Yao, A review of the preparation, properties and applications of VO_2 thin films with the reversible phase transition, Front. Mater. 11 (2024) 1341518, https://doi.org/10.3389/fmats.2024.1341518.

[8] Y. Wang, E.L. Runnerstrom, D.J. Milliron, Switchable Materials for Smart Windows, Annu. Rev. Chem. Biomol. Eng. 7 (2016) 283–304, https://doi.org/10.1146/annurev-chembioeng-080615-034647.

[9] N. DeForest, A. Shehabi, J. O'Donnell, G. Garcia, J. Greenblatt, E.S. Lee, S. Selkowitz, D.J. Milliron, United States energy and CO_2 savings potential from deployment of near-infrared electrochromic window glazings, Build. Environ. 89 (2015) 107–117, https://doi.org/10.1016/j.buildenv.2015.02.021.

[10] T.D. Vu, S. Liu, X. Zeng, C. Li, Y. Long, High-power impulse magnetron sputtering deposition of high crystallinity vanadium dioxide for thermochromic smart windows applications, Ceram. Int. 46 (2020) 8145–8153, https://doi.org/10.1016/j.ceramint.2019.12.042.

[11] H. Song, H. Li, X. Ma, G. Yin, Thermochromic performance enhancement by geometric structure optimization of VO_2 nanoarrays for smart window application, Opt. Commun. 546 (2023) 129763, https://doi.org/10.1016/j.optcom.2023.129763.

[12] M. Li, Y. Cheng, C. Fang, X. Zhang, H. Han, Y. Zhang, Recent advances in vanadium dioxide for dynamic thermal radiation modulation: a review, Sol. Energy Mater. Sol. Cells 275 (2024) 113040, https://doi.org/10.1016/j.solmat.2024.113040.

[13] C. Geng, M. Zhang, H. Wei, J. Gu, T. Zhao, H. Guan, S. Liang, O. Boytsova, S. Dou, Y. Chen, Y. Li, Z. Tian, Tracking the optical constants of self-patterned VO_2-based on smart windows during metal-insulator transition, Sol. Energy Mater. Sol. Cells 272 (2024) 112892, https://doi.org/10.1016/j.solmat.2024.112892.

[14] Y. Gao, H. Luo, Z. Zhang, L. Kang, Z. Chen, J. Du, M. Kanehira, C. Cao, Nanoceramic VO_2 thermochromic smart glass: a review on progress in solution processing, Nano Energy 1 (2012) 221–246, https://doi.org/10.1016/j.nanoen.2011.12.002.

[15] F.J. Morin, Oxides which show a metal-to-insulator transition at the neel temperature, Phys. Rev. Lett. 3 (1959) 34–36, https://doi.org/10.1103/PhysRevLett.3.34.

[16] H. Yoon, M. Choi, T.W. Lim, H. Kwon, K. Ihm, J.K. Kim, S.Y. Choi, J. Son, Reversible phase modulation and hydrogen storage in multivalent VO_2 epitaxial thin films, Nat. Mater. 15 (2016) 1113–1119, https://doi.org/10.1038/nmat4692.

[17] S. Liang, Q. Shi, H. Zhu, B. Peng, W. Huang, One-step hydrothermal synthesis of W-Doped VO_2 (M) nanorods with a tunable phase-transition temperature for infrared smart windows, ACS Omega 1 (2016) 1139–1148, https://doi.org/10.1021/acsomega.6b00221.

[18] H. Zong, H. Chen, L. Bian, B. Sun, Y. Yin, C. Zhang, W. Qiao, L. Yan, Q. Hu, M. Li, An approach for obtaining thermochromic smart windows with excellent performance and low phase transition temperature based on VO_2/tungsten-doped VO_2/VO_2 composite structure, Infrared Phys. Technol. 137 (2024) 10518, https://doi.org/10.1016/j.infrared.2024.105186.

[19] Z. Xiang, Z. Wu, Y. Shi, C. Li, X. Chen, J. Gou, J. Wang, Y. Zhuang, X. Dong, X. Zheng, Y. Jiang, Optimized thermochromic properties for smart window application of VO_2 films by wet-etching process, Opt. Mater. 128 (2022) 112359, https://doi.org/10.1016/j.optmat.2022.112359.

[20] J. Pi, C.B. Li, R.Y. Sun, L.Y. Li, F. Wang, F. Song, J.M. Wu, X.L. Wang, Y.Z. Wang, Superhydrophobic and thermochromic VO_2-based composite coatings for energy-saving smart windows, Compos. Commun. 32 (2022) 101167, https://doi.org/10.1016/j.coco.2022.101167.

[21] J.M.C. Puguan, P.V. Rathod, P.V. Chavan, J. Lee, H. Kim, Solar light modulating materials for energy efficient smart window design: recent trends and future perspectives, Sol. Energy Mater. Sol. Cells 282 (2025) 113407, https://doi.org/10.1016/j.solmat.2025.113407.

[22] S. Bhupathi, S. Wang, Y. Ke, Y. Long, Recent progress in vanadium dioxide: the multi-stimuli responsive material and its applications, Mater. Sci. Eng. R. Rep. 155 (2023) 100747, https://doi.org/10.1016/j.mser.2023.100747.

[23] S. Wang, M. Liu, L. Kong, Y. Long, X. Jiang, A. Yu, Recent progress in VO_2 smart coatings: strategies to improve the thermochromic properties, Prog. Mater. Sci. 81 (2016) 1–54, https://doi.org/10.1016/j.pmatsci.2016.03.001.

[24] L. Chen, H. Hu, Y. Cui, Y. Gao, Continuously tunable the phase transition behavior of VO_2 by T-doping and the formation of T-T chain (T = Ta, Nb), Ceram. Int. 50 (2024) 6543–6556, https://doi.org/10.1016/j.ceramint.2023.11.400.

[25] Z. Shao, X. Cao, H. Luo, P. Jin, Recent progress in the phase-transition mechanism and modulation of vanadium dioxide materials, NPG Asia Mater. 10 (2018) 581–605, https://doi.org/10.1038/s41427-018-0061-2.

[26] A. Romanyuk, R. Steiner, L. Marot, P. Oelhafen, Temperature-induced metal-semiconductor transition in W-doped VO_2 films studied by photoelectron spectroscopy, Sol. Energy Mater. Sol. Cells 91 (2007) 1831–1835, https://doi.org/10.1016/j.solmat.2007.06.013.

[27] M. Kong, K. Egbo, C.P. Liu, M.K. Hossain, C.Y. Tso, C.Y. Hang Chao, K.M. Yu, Rapid thermal annealing assisted facile solution method for tungsten-doped vanadium dioxide thin films on glass substrate, J. Alloys Compd. 833 (2020) 155053, https://doi.org/10.1016/j.jallcom.2020.155053.

[28] B. Li, S. Tian, Z. Wang, B. Liu, X. Gong, X. Zhao, Thermochromic Ta doped VO_2 films: enhanced luminous transmittance, significantly depressed phase transition temperature and hysteresis width, Appl. Surf. Sci. 568 (2021) 150959, https://doi.org/10.1016/j.apsusc.2021.150959.

[29] J. Li, N. Yuan, T. Xie, D. Dan, Influence of Ta doping on the phase transition characteristics of VO_2 polycrystalline thin films, in: Proc. SPIE, 2nd Int. Symp. Adv. Opt. Manuf. Test. Technol. Adv. Opt. Manuf. Technol., 2006 61490B, https://doi.org/10.1117/12.674198.

[30] D. Kang, J. Kim, M. Lee, High-quality VO_2 thin films sputter-deposited on borosilicate glass substrates for modulating solar transmission and thermal emission, J. Alloys Compd. 1008 (2024) 176793, https://doi.org/10.1016/j.jallcom.2024.176793.

[31] V. Collado, N. Martin, P. Pedrosa, J.Y. Rauch, M. Horakova, M.A.P. Yazdi, A. Billard, Temperature dependence of electrical resistivity in oxidized vanadium films grown by the GLAD technique, Surf. Coat. Technol. 304 (2016) 476–485, https://doi.org/10.1016/j.surfcoat.2016.07.057.

[32] Y.X. Ji, G.A. Niklasson, C.G. Granqvist, M. Boman, Thermochromic VO_2 films by thermal oxidation of vanadium in SO_2, Sol. Energy Mater. Sol. Cells 144 (2016) 713–716, https://doi.org/10.1016/j.solmat.2015.10.012.

[33] Y. Xue, S. Yin, Element doping: a marvelous strategy for pioneering the smart applications of VO_2, Nanoscale 14 (2022) 11054–11097, https://doi.org/10.1039/d2nr01864k.

[34] A.J. Santos, N. Martin, J. Outón, E. Blanco, R. García, F.M. Morales, A simple two-step approach to the fabrication of VO_2-based coatings with unique thermochromic features for energy-efficient smart glazing, Energy Build. 285 (2023) 112892, https://doi.org/10.1016/j.enbuild.2023.112892.

[35] A.J. Santos, N. Martin, J. Outón, E. Blanco, R. García, F.M. Morales, Towards the optimization of a simple route for the fabrication of energy-efficient VO_2-based smart coatings, Sol. Energy Mater. Sol. Cells 254 (2023) 112253, https://doi.org/10.1016/j.solmat.2023.112253.

[36] A.J. Santos, N. Martin, J.J. Jiménez, R. García, F.M. Morales, Enhancing luminous transmittance and hysteresis width of VO_2-based thermochromic coatings by combining GLAD and RGPP approaches, Constr. Build. Mater. 419 (2024) 135472, https://doi.org/10.1016/j.conbuildmat.2024.135472.

[37] A.J. Santos, A. Casas-Acuña, N. Martin, J.J. Jiménez, A. Krystianiak, O. Heintz, R. García, F.M. Morales, Energy-efficient W-doped VO_2-based smart glasses by glancing angle co-deposition and subsequent rapid thermal annealing, Results Eng. 27 (2025) 106323, https://doi.org/10.1016/j.rineng.2025.106323.

[38] H. Sun, D. Chen, L. Zhou, W. Mi, D. Wang, L. He, J. Zhao, The synergistic effect of Ta-doping and antireflective TaO_x layer on the thermochromic VO_2 thin films for smart windows, Sol. Energy Mater. Sol. Cells 275 (2024) 113010, https://doi.org/10.1016/j.solmat.2024.113010.

[39] W. Xu, Z. Wu, Z. Xiang, J. Gou, X. Dong, J. Wang, Y. Jiang, Vanadium oxide thin films with extremely narrow thermal hysteresis loop width were obtained by Ta doping for THz modulation applications, Opt. Mater. 117 (2021) 111142, https://doi.org/10.1016/j.optmat.2021.111142.

[40] A.J. Santos, B. Lacroix, M. Domínguez, R. García, N. Martin, F.M. Morales, Controlled grain-size thermochromic VO_2 coatings by the fast oxidation of sputtered vanadium or vanadium oxide films deposited at glancing angles, Surf. Interfaces 27 (2021) 101581, https://doi.org/10.1016/j.surfin.2021.101581.

[41] A.J. Santos, N. Martin, J.J. Jiménez, R. Alcántara, S. Margueron, A. Casas-Acuña, R. García, F.M. Morales, Facile fabrication of high-performance thermochromic VO_2 -based films on Si for application in phase-change devices, Chem. Mater. 35 (2023) 4435–4448, https://doi.org/10.1021/acs.chemmater.3c00613.

[42] J. Outón, E. Blanco, M. Domínguez, H. Bakkali, J.M. Gonzalez-Leal, J.J. Delgado, M. Ramírez-del-Solar, Tracking the optical constants of porous vanadium dioxide thin films during metal–insulator transition: Influence of processing conditions on their application in smart glasses, Appl. Surf. Sci. 580 (2022) 152228, https://doi.org/10.1016/j.apsusc.2021.152228.

[43] T.C. Chang, X. Cao, S.H. Bao, S.D. Ji, H.J. Luo, P. Jin, Review on thermochromic vanadium dioxide based smart coatings: from lab to commercial application, Adv. Manuf. 6 (2018) 1–19, https://doi.org/10.1007/s40436-017-0209-2.
[44] A.E. Ersundu, M. Çelikbilek Ersundu, E. Doğan, M.B. Güven, A comparative investigation on thermal, structural and optical properties of W and Nb-doped VO_2-based thermochromic thin films, Thin Solid Films 700 (2020) 137919, https://doi.org/10.1016/j.tsf.2020.137919.
[45] H. Wada, T. Fukawa, K. Toyota, K. Koike, M. Kawahara, Lowering of phase transition temperature for Nb or Ta doped VO_2 thin films grown by MOD, IEEJ Trans. Fundam. Mater. 142 (5) (2021) 221–228, https://doi.org/10.1541/ieejfms.142.221.
[46] M.M. Margoni, S. Mathuri, K. Ramamurthi, R.R. Babu, K. Sethuraman, Sprayed vanadium pentoxide thin films: Influence of substrate temperature and role of HNO_3 on the structural, optical, morphological and electrical properties, Appl. Surf. Sci. 418 (2017) 280–290, https://doi.org/10.1016/j.apsusc.2017.02.039.
[47] A. Baltakesmez, C. Aykaç, B. Güzeldir, Phase transition and changing properties of nanostructured V_2O_5 thin films deposited by spray pyrolysis technique, as a function of tungsten dopant, Appl. Phys. A Mater. Sci. Process. 125 (2019) 441, https://doi.org/10.1007/s00339-019-2736-0.